Domain Wall Propagation through Spin Wave Emission

X. S. Wang,[1] P. Yan,[2] Y. H. Shen,[1] G. E. W. Bauer,[3,2] and X. R. Wang[4,1,*]

[1]*Physics Department, The Hong Kong University of Science and Technology, Clear Water Bay, Kowloon, Hong Kong*
[2]*Kavli Institute of NanoScience, Delft University of Technology, Lorentzweg 1, 2628 CJ Delft, Netherlands*
[3]*Institute for Materials Research, Tohoku University, Sendai 980-8577, Japan*
[4]*School of Physics, Wuhan University, Wuhan, People's Republic of China*

(Received 27 May 2012; published 18 October 2012)

We theoretically study field-induced domain wall motion in an electrically insulating ferromagnet with hard- and easy-axis anisotropies. Domain walls can propagate along a dissipationless wire through spin wave emission locked into the known soliton velocity at low fields. In the presence of damping, the usual Walker rigid-body propagation mode can become unstable for a magnetic field smaller than the Walker breakdown field.

DOI: 10.1103/PhysRevLett.109.167209 PACS numbers: 75.60.Jk, 75.30.Ds, 75.60.Ch, 85.75.−d

Magnetic domain wall (DW) propagation in nanowires has attracted attention because of the academic interest of a unique nonlinear system [1–4] and potential applications in data storage and logic devices [4–6]. The field-driven DW dynamics is governed by the Landau-Lifshitz-Gilbert (LLG) equation [1], which has analytical solutions in limiting cases [1,7], such as the soliton solution [8] in the absence of both dissipations and external magnetic fields. The interplay between spin waves (SWs) and DWs has also received attention, including DW propagation driven by externally generated SWs [9–11] and SW generation by a moving DW [12,13]. Our understanding of the field-induced DW motion is nevertheless far from complete. According to conventional wisdom, DWs move under a static magnetic field only in the presence of energy dissipation [1,14]. Numerical evidence against this view therefore came as a surprise [12,15].

We report here a physical picture for the SW emission-induced domain wall motion for a head-to-head DW in a magnetic nanowire with the easy axis along the wire (z direction) as shown in Fig. 1. Let $K_\parallel$ and $K_\perp$ be anisotropy coefficients of the easy and hard axis (along the x direction), respectively. An external field along the wire rotates the DW out of the yz plane. The DW structure thereby experiences an internal field in the x direction twisting the DW plane and generating a nonuniform internal field along the wire. This field causes periodic deformations of the DW structure, such as "breathing" [1] by which the entire DW precesses around the wire axis while its width shrinks and expands periodically. The local modulation of the magnetization texture generates SWs (wavy lines with arrows in Fig. 1) that radiate away from the DW center. The energy needed to generate the SWs has to come from the Zeeman energy [14] that is released by propagating the DW. The DW velocity of a dissipationless ferromagnet in the steady state may then be expected to be proportional to the SW emission rate.

In this Letter, we numerically solve the LLG equation, initially without damping in order to confirm the above mentioned relation between spin wave emission and DW propagation. Depending on $K_\perp$ and the magnetic field, breathing or more complicated periodic transformations of the DW emit spin waves. The DW propagation at low fields tends to lock into a particular soliton mode in which the energy dissipation rate due to the SW emission is balanced by the Zeeman energy gain. We predict robust spin wave emission that persists in the presence of Gilbert damping and renders the usual Walker rigid-body propagation mode unstable in a region below the Walker breakdown field.

The LLG equation reads

$$\frac{\partial \mathbf{m}}{\partial t} = -\mathbf{m} \times \mathbf{h}_{\text{eff}} + \alpha \mathbf{m} \times \frac{\partial \mathbf{m}}{\partial t}, \tag{1}$$

where $\mathbf{m}$ is the unit direction of the local magnetization $\mathbf{M} = \mathbf{m}M_s$ with saturation magnetization M_s and α is the Gilbert damping constant. The effective magnetic field of our wire with biaxial magnetic anisotropy (see Fig. 1) is $\mathbf{h}_{\text{eff}} = K_\parallel m_z \hat{z} - K_\perp m_x \hat{x} + A\nabla^2 \mathbf{m} + H\hat{z}$, consisting of internal and external fields in units of M_s. A is the exchange constant. In a narrow stripe whose width and thickness do

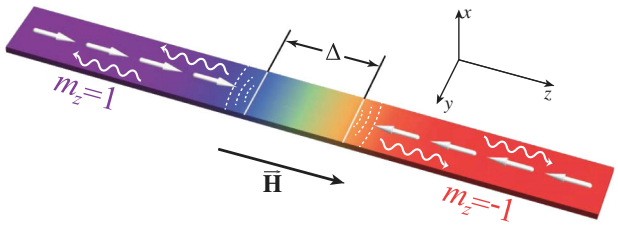

FIG. 1 (color online). Schematic transverse head-to-head DW of width Δ in a magnetic nanowire. $\vec{\mathbf{H}}$ is an external field along the wire axis defined as the z direction. DW breathing and other types of periodic DW deformations emit spin waves, denoted by the wavy lines with arrows.

not exceed the exchange length, the exchange interaction dominates the stray field energy caused by magnetic charges on the edges; the DW structure tends to be homogeneous in the transverse direction [15], i.e., behaves effectively one-dimensional (1D). Time, length, and energy density are measured in units of $(\gamma M_s)^{-1}$ with gyromagnetic ratio γ, the DW width at equilibrium $\Delta_0 = \pi\sqrt{A/K_\parallel}$, and $\mu_0 M_s^2$, respectively. We chose parameters of the electric insulator yttrium iron garnet (YIG) with [11,16] $A = 3.84 \times 10^{-12}$ J/m, $K_\parallel = 2 \times 10^3$ J/m^3, $\gamma = 35.1$ kHz/(A/m), and $M_s = 1.94 \times 10^5$ A/m. The corresponding units of time and length are 1.46×10^{-10} s and 1.38×10^{-7} m, respectively. $K_\perp$ and α are treated as adjustable parameters depending on the sample shape and microscopic order. We solve Eq. (1) by a numerically stable method [17]. The mesh size is chosen to be 0.009, corresponding to the YIG lattice constant (1.24 nm).

In order to prove that a DW under an external field indeed emits spin waves, we plot snapshots of the distribution of $m_\perp \equiv \sqrt{m_x^2 + m_y^2}$ for $K_\perp = 4$ and 10 (in units of $\mu_0 M_s^2$), $\alpha = 0$, and $H = 0.01$ (for $t > 0$) at various times in Figs. 2(a) and 2(b). At $t = 0$, right before the external field is switched on, $m_\perp$ follows the Walker DW profile [1], and the DW is centered at $z = 0$ in a wire with length $180\Delta_0$, while the DW magnetization lies in the yz plane. Curves are offset for better visibility. As time proceeds ($t > 0$), SWs (wavy features) are emitted into both directions, while the DW center (peak) moves simultaneously along the field slower than the SWs. The velocity v for a fixed magnetic field increases monotonically with $K_\perp$ (Fig. 3). It does not depend sensitively on small $K_\perp (<4)$ but grows rapidly when $K_\perp$ is close to 8 and becomes an almost linear function for $K_\perp > 12$. From the time dependence of the position (dashed lines) of the DW center and azimuthal angle (solid lines) shown in the insets of Fig. 3 for a small and large $K_\perp$, we trace the periodic DW deformations in the different field regions. We note that such a large $K_\perp$ value may be realized in YIG samples subject to mechanical strains [18].

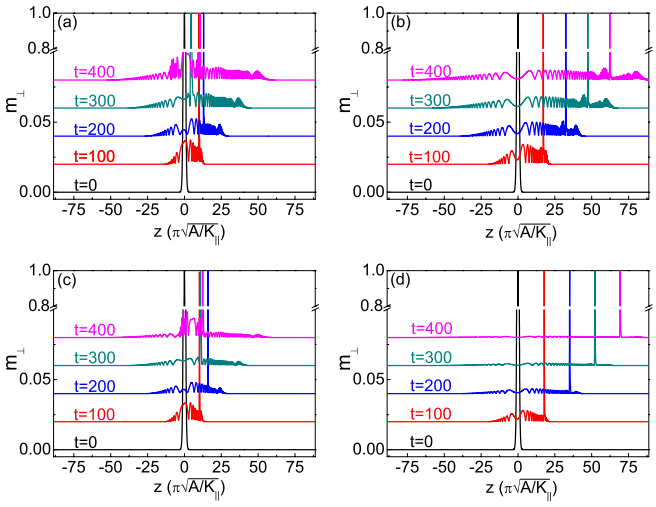

FIG. 2 (color online). Snapshots of $m_\perp = \sqrt{m_x^2 + m_y^2}$ for $H = 0.01$ at various times t for (a) $K_\perp = 4$ and $\alpha = 0$; (b) $K_\perp = 10$ and $\alpha = 0$; (c) $K_\perp = 4$ and $\alpha = 0.001$; and (d) $K_\perp = 10$ and $\alpha = 0.001$.

At a small $K_\perp = 4$ (left inset), **m** at the DW center rotates around the wire, while the center position oscillates back and forth but also moves slowly along the applied field. This oscillatory motion is synchronized with the breathing, i.e., the periodic energy absorption and release in the form of periodic oscillation of the DW width $\Delta = \pi\sqrt{A/(K_\parallel + K_\perp \cos^2\phi)}$ [1], where ϕ is the tilt angle of the DW plane (with equilibrium value $\pi/2$). This breathing excites spin waves as shown in Fig. 2(a). Low velocities correspond to weak SW emission. At a large $K_\perp = 10$ (right inset), the azimuthal angle of the DW center approaches a fixed value, and the DW center position moves at a constant velocity, since ϕ and the DW energy are almost constant. In this case, **m** still rotates around the wire axis, while the DW center propagates along the wire with a fixed ϕ. The large $K_\perp$ twists the DW plane into a chiral screwlike structure that changes shape periodically during the magnetization precession while the DW center "drills" forward. This drilling mode is much more efficient in emitting SWs than the breathing mode, leading to a relatively high DW propagating speed. For YIG parameters the SW velocity exceeds that of the DW; therefore, in contrast with Ref. [12], we observe bow as well as stern SW excitations.

Figure 4(a) displays the steady state DW velocity in a dissipationless wire with $K_\perp = 4$, 10, and 16 with parameters otherwise identical to those of Fig. 3. As a function of field it increases abruptly for small values, reaches a maximal value, and decreases again. When $K_\perp$ is reduced from

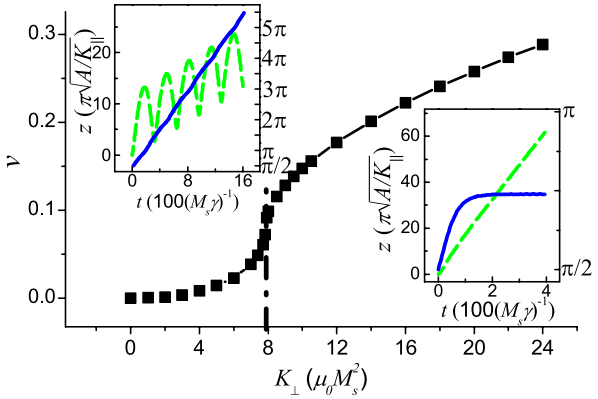

FIG. 3 (color online). $K_\perp$ dependence of the DW velocity v (in units of $\pi\gamma M_s\sqrt{A/K_\parallel}$) for fixed $H = 0.01$ and $\alpha = 0$. Insets: Time dependence of the DW center position (dashed line) and the azimuthal angle ϕ (solid line) of magnetization at the DW center for $K_\perp = 4$ (left) and $K_\perp = 10$ (right).

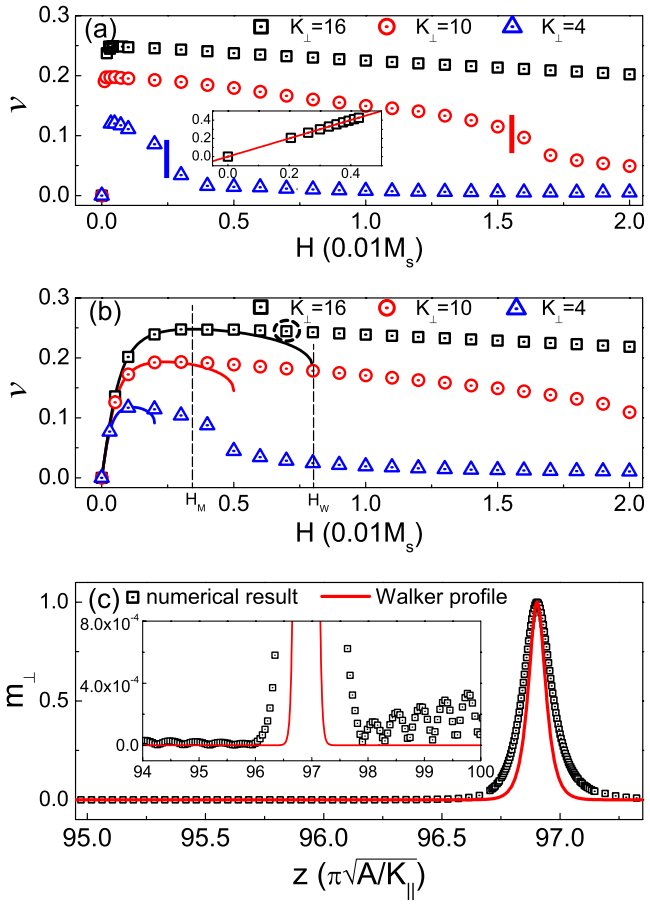

FIG. 4 (color online). (a), (b) Field dependence of DW velocity for various $K_\perp$. Field and velocity are in units of $0.01M_s$ and $\pi\sqrt{A/K_\parallel}\gamma M_s$, respectively. A, $K_\parallel$, and M_s are YIG parameters. (a) $\alpha = 0$. Inset: Symbols display $-\sin 2\phi$ vs $v\sqrt{(K_\parallel + K_\perp \cos^2\phi)/A/K_\perp}$, where v is the soliton velocity. The line is the linear relationship from soliton theory. (b) $\alpha = 0.001$. The solid curves are the corresponding Walker solutions. (c) Snapshot of $m_\perp$ for $H = 0.007$ and $K_\perp = 16$ at $t = 400$ [for the data point indicated by a circle in (b)]. The numerical results deviate from the Walker profile that is clearly narrower. Inset: Expanded view of $m_\perp$ close to the DW center. The relative deviation from the Walker profile (solid curve) is pronounced and spin wave emission is conspicuous.

16 to 4, the DW changes from drilling to breathing motion, resulting in a significant drop of DW velocity. The decrease of DW velocity with field should not be interpreted as suppression of DW propagation by the damping due to spin wave emission [12,19]. The Zeeman energy released by the DW motion at a rate $2HMv$ [14] should be equal to the energy rate carried away by the SWs. Therefore, provided that the latter increases sublinearly with H ($\propto H^\beta$ and $\beta < 1$), the DW propagation speed must decrease with field. The initial rapid rise of the DW velocity at small fields is related to the soliton solution $\ln\tan(\theta/2) = \pi(z - vt)/\Delta$ of the LLG Eq. (1) with soliton velocity $v = -\sqrt{A/(K_\parallel + K_\perp\cos^2\phi)K_\perp}\sin 2\phi$ for $\alpha = 0$ and $H = 0$ [8], where θ is the polar angle of $\mathbf{m}$. This can be seen from the plot of $-\sin 2\phi$ for the saturated ϕ vs $v\sqrt{(K_\parallel + K_\perp\cos^2\phi)/A/K_\perp}$ (symbols) for $H \in [0, 0.0009]$ in the inset in Fig. 4(a) for $K_\perp = 16$. The numerical data agree precisely with the soliton velocity formula (solid line). Since conventional solitons do not satisfy the LLG equation in the presence of an external field, we unearthed here a hybridized mode of solitons and spin waves. In contrast to the zero field case, there is only one particular soliton mode in which the SW emission is balanced by the Zeeman energy change, viz. the moving DW. This holds as long as the field is smaller than the value at which $-\sin 2\phi$ reaches its maximum value 1. Beyond that field, the soliton mode becomes instable, since the SW emission rate cannot keep up with the released Zeeman energy and other propagation modes have to take over. This soliton instability point is emphasized by vertical bars in the data points for $K_\perp = 4$ and $K_\perp = 10$, indicating the threshold fields below which the soliton formula holds. For $K_\perp = 16$ this value is out of the range of Fig. 4(a).

For YIG parameters and $K_\perp = 10$, the DW velocity at $H = 0.01(\sim 24$ Oe) is about 140 m/s. For comparison, the corresponding DW velocity by Walker rigid-body propagation for the same parameters and $\alpha = 0.05$ is 57 m/s [1]. We may conclude that the DW velocity in weakly dissipative magnetic insulators is of the same order of magnitude as in highly dissipative ferromagnetic metals.

DW propagation through spin wave emission exists in any magnetic wire with transverse magnetic anisotropy irrespective of the Gilbert damping. Figures 2(c) and 2(d) look very similar to Figs. 2(a) and 2(b) in spite of the finite damping $\alpha = 0.001$. Naturally, in the presence of damping the SWs can propagate only over finite distances, which explains why they have been overlooked in most experimental and numerical studies. In Figs. 2(b) (or 2(a)) and 2(d) (or 2(c)), the DW velocity is higher in the presence of a small nonzero damping, since damping dissipates an energy on top of the SW emission and the DW velocity is proportional to the energy dissipation rate [14]. Here we find a mixed DW propagation mode that profits from both Gilbert damping and spin wave emission. Figure 4(b) is the field dependence of the DW velocity for $\alpha = 0.001$ and various $K_\perp$, while other model parameters are unmodified from Fig. 4(a). Except at very small fields, Fig. 4(b) is similar to Fig. 4(a). The numerically obtained velocities (symbols) in Fig. 4(b) agree well with Walker's rigid-body propagation (solid curves) [1,13] below some maximum field $H_M \simeq 2(K_\parallel/K_\perp)^{0.25}H_W$ for $K_\perp \gg K_\parallel$, where $H_W = \alpha K_\perp/2$ [1] is the Walker breakdown field. However, deviations are obvious for fields between H_M and H_W (where the solid lines end). This implies that Walker rigid-body propagation is not stable for $H \in [H_M, H_W]$ with respect to the spin wave emission mode.

In order to prove numerically that the Walker solution is stable only for $H < H_M$, we solve the LLG Eq. (1) by starting from an initial magnetization configuration that deviates slightly from the rigid-body propagation mode. The magnetization indeed converges to the Walker profile for $H < H_M$. However, this changes when we consider $H = 0.007$ for $K_\perp = 16$ [indicated by dashed circle in Fig. 4(b)] with all other parameters the same. According to Walker theory [1], $H_M = 0.00344$ and $H_W = 0.008$ [indicated by dashed lines in Fig. 4(b)]. The symbols in Fig. 4(c) give a snapshot of $m_\perp$ for $t = 400$, at which the transients die out and the DW center propagates to about $z = 97$. The distribution deviates significantly from the Walker profile (solid curve). The spin wave emission is clearly observed in the expanded tail in the inset in Fig. 4(c).

There are several corollaries of the DW propagation mode by spin wave emission. The emitted spin waves from one DW, for example, can mediate an attractive force on a nearby DW by spin transfer [11]. This causes cross talk in wires with more than one DW with consequences for the ''racetrack'' memory [4]. This DW-DW attractive force has a finite range governed by the Gilbert damping and is sensitive to material parameters and geometry. The increase of the effective damping by SW emission [19] is not restricted to DWs but will appear in any time-dependent magnetization texture including magnetic vortices and cannot be captured by the Gilbert phenomenology. On the other hand, our results possibly open alternatives to manipulate and control the effective damping in magnetic nanostructures. In contrast to what has been reported earlier [12,15], we not only observe SW assisted DW propagation but also reveal the underlying physical principles. The present results have been obtained in the limit of narrow wires, in which the domain wall texture is simply transverse and the spin waves escape only in one direction. In extended films, the domain walls contain vortices and display more complex propagation patterns, while the spin waves can be emitted in all directions. A detailed study of this experimentally relevant regime should be of considerable interest.

In conclusion, we reveal the physical nature of the DW propagation through spin wave emission and give a mathematical description of the motion in terms of hybridized SW and soliton solutions. We prove that a DW in a wire with a finite transverse magnetic anisotropy undergoes a periodic transformation under an external magnetic field that excites SWs. The energy carried away must be compensated by the Zeeman energy that is released by DW propagation along the wire. The DW propagation adopts one particular soliton velocity at low fields. This SW assisted DW propagation can be attributed to the SW emission generated by DW breathing and drilling modes. In the presence of damping it competes with and appears before the Walker breakdown. Also, the spin wave emission will mediate a dynamic attractive force between DWs with a range controlled by the Gilbert damping.

This work is supported by Hong Kong UGC/CERG grants (No. 604109, No. HKUST17/CRF/08, and No. RPC11SC05), the FOM foundation, DFG Priority Program SpinCat, and EG-STREP MACALO.

*phxwan@ust.hk

[1] N. L. Schryer and L. R. Walker, J. Appl. Phys. **45**, 5406 (1974).
[2] D. A. Allwood, G. Xiong, C. C. Faulkner, D. Atkinson, D. Petit, and R. P. Cowburn, Science **309**, 1688 (2005).
[3] G. S. D. Beach, C. Knutson, C. Nistor, M. Tsoi, and J. L. Erskine, Phys. Rev. Lett. **97**, 057 203 (2006).
[4] S. S. P. Parkin, M. Hayashi, and L. Thomas, Science **320**, 190 (2008).
[5] G. Malinowski, O. Boulle, and M. Kläui, J. Phys. D **44**, 384 005 (2011); C. H. Marrows and G. Meier, J. Phys. Condens. Matter **24**, 020 301 (2012); G. Tatara, H. Kohno, and J. Shibata, Phys. Rep. **468**, 213 (2008).
[6] R. Nebashi, N. Sakimura, Y. Tsuji, S. Fukami, H. Honjo, S. Saito, S. Miura, N. Ishiwata, K. Kinoshita, T. Hanyu, T. Endoh, N. Kasai, H. Ohno, and T. Sugibayashi, in *Proceedings of the IEEE Symposium on VLSI Circuits*, Digest of Technical Paper 300 (IEEE, New York, 2011).
[7] Z. Z. Sun and X. R. Wang, Phys. Rev. Lett. **97**, 077 205 (2006); X. R. Wang and Z. Z. Sun, *ibid.* **98**, 077 201 (2007).
[8] H. B. Braun, Adv. Phys. **61**, 1 (2012).
[9] D. S. Han, S. K. Kim, J. Y. Lee, S. J. Hermsoerfer, H. Schutheiss, B. Leven, and B. Hillebrands, Appl. Phys. Lett. **94**, 112 502 (2009).
[10] S. M. Seo, H. W. Lee, H. Kohno, and K. J. Lee, Appl. Phys. Lett. **98**, 012 514 (2011).
[11] P. Yan, X. S. Wang, and X. R. Wang, Phys. Rev. Lett. **107**, 177 207 (2011).
[12] R. Wieser, E. Y. Vedmedenko, and R. Wiesendanger, Phys. Rev. B **81**, 024 405 (2010).
[13] M. Yan, C. Andreas, A. Kákay, F. García-Sánchez, and R. Hertel, Appl. Phys. Lett. **99**, 122 505 (2011).
[14] X. R. Wang, P. Yan, J. Lu, and C. He, Ann. Phys. (N.Y.) **324**, 1815 (2009); X. R. Wang, P. Yan, and J. Lu, Europhys. Lett. **86**, 67 001 (2009).
[15] D. G. Porter and M. J. Donahue, J. Appl. Phys. **95**, 6729 (2004).
[16] H. Kurebayashi, O. Dzyapko, V. E. Demidov, D. Fang, A. J. Ferguson, and S. O. Demokritov, Nature Mater. **10**, 660 (2011).
[17] X. P. Wang, C. J. García-Cervera, and W. E, J. Comput. Phys. **171**, 357 (2001).
[18] A. Hubert and R. Schäfer, *Magnetic Domains* (Springer, Heidelberg, 1998).
[19] D. Bouzidi and H. Suhl, Phys. Rev. Lett. **65**, 2587 (1990).